AIAA Journal

VOLUME 8 NOVEMBER 1970 NUMBER 11

Compressible Laminar Boundary Layer on a Cone at High Angle of Attack

RUSSELL A. SMITH* AND PAUL K. CHANG†
The Catholic University of America, Washington, D. C.

An approximate integral method is applied to the three-dimensional laminar boundary-layer equations, including the energy equation for Prandtl number equal to unity, to obtain a solution to the attached boundary layer on slender cones in hypersonic flight at high angles of attack. The velocity and total enthalpy profiles are of the Timman type. The crossflow velocity profile is a two-parameter family allowing for nonzero crossflow at streamline inflection points. Because of the high angles of attack considered, the solution includes the effect of large crossflow velocity on the boundary layer. Using the pressure data available in the literature, results for the heat transfer coefficient, surface shear stress direction, and position of separation are computed. The computations compare favorably with data from the literature.

Nomenclature

C = const in temperature-viscosity relation $\mu/\mu_e = CT/T_e$
c_f = surface shear stress divided by $\rho_o u_o^2/2$
G = pressure gradient parameter, $(dp/d\phi)/\gamma p M^2$
$F(M)$ = $(\gamma - 1)M^2/2$
H = total enthalpy
h_1,h_2 = scale factors in equation of motion, Eq. (1)
K_1,K_2 = curvature terms used in Eq. (1)
l,m = direction cosines of inviscid streamline tangent
M = Mach number at edge of boundary layer
$p,\bar{p}$ = static pressure, and dimensionless static pressure ratio p/p_o
R = radius measured from cone tip
Re = Reynolds number, $\rho_o u_o R/\mu_o$
S = total enthalpy parameter, $H/H_e - 1$
St = Stanton number, wall heat flux rate divided by $\rho_o u_o(H_e - H_w)$
T = absolute static temperature
u,v,w = velocity components in ξ, η, ζ directions, respectively
$\bar{u}$ = dimensionless velocity ratio, u/u_o
Y = Parameter in Appendix B, $-(1 + S_w)[1 + (\gamma - 1)M^2/2]G\bar{u}/\bar{p}$
z = dimensionless distance used in profiles, Eqs. (8) and (9)
α = angle of attack
γ = ratio of specific heats
δ = boundary-layer thickness
$\delta_1,\bar{\delta}_{11}$, etc. = thickness parameters defined in Appendix A in transformed coordinates
δ_1,θ_{11}, etc. = thickness parameters defined in Appendix A in physical coordinates
Δ = three-dimensional displacement thickness
η^k = unit vector tangent to streamline normal coordinate
λ^k = unit vector tangent to streamline coordinate
μ = absolute viscosity
ν = kinematic viscosity
ξ,η,ζ = streamline coordinates, see Fig. 1
Π = free parameter in crossflow velocity profile, Eq. (8b)
$\rho,\bar{\rho}$ = density, and dimensionless density ratio ρ/ρ_o
σ = free parameter used in defining dimensionless distance, z
Σ = $\sigma u_o/R$
ϕ = azimuthal angle measured from windward meridian
χ = free parameter in total enthalpy profile, Eq. (9)

Subscripts

e = indicates edge of boundary layer
o = indicates edge of boundary layer at windward meridian
w = indicates surface or wall value

Received August 21, 1969; revision received January 20, 1970. This research was sponsored by the Advanced Research Projects Agency/Department of the Army, Washington, D.C., under Contract N-00017-67-C-0008.

* Assistant Professor of Mechanical Engineering, Member AIAA.
† Professor of Mechanical Engineering. Associate Fellow AIAA.

Introduction

HIGH-SPEED slender cone-shaped vehicles, whether of the lifting re-entry class or maneuverable interceptors, can encounter flight conditions of very high angle of attack. The aerodynamic problem for such a vehicle is complicated by the interaction of an inviscid flowfield, a large separated region on the leeward side, and an attached three-dimensional boundary layer. The attached boundary-layer computations provide information such as the local heat-transfer rate and also initial values for the computation of the separated flow region on the leeward side.

The boundary layer is greatly influenced by the crossflow. This crossflow, which is identically zero at the windward meridian, grows along the streamwise direction under

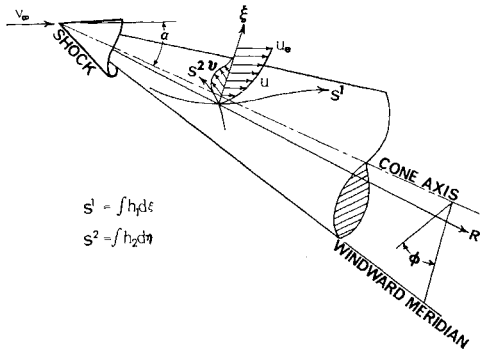

Fig. 1 Streamline coordinates for three-dimensional boundary layer.

the influence of a transverse pressure gradient. In the region of the pressure minimum the magnitude of the crossflow was found to be comparable to the streamwise velocity, even at angles of attack on the order of one cone half angle. By avoiding simplifying assumptions such as similar profiles and small crossflow velocity, special emphasis was placed in this analysis on the large crossflow and the determination of properties up to the separation point.

As sketched in Fig. 1, an orthogonal streamline coordinate system was formed from the inviscid surface streamlines, the normals to the streamline in the cone-surface, and the surface normals. The crossflow is less pronounced in such a coordinate system because of the zero boundary conditions imposed on the crossflow velocity profile at the wall and the free stream. The strength or magnitude of the crossflow is conveniently measured by the ratio of the crossflow wall shear stress to the streamwise wall shear stress or by the angle between the resultant wall shear stress and the inviscid streamline direction. If this angle is small, the crossflow velocity is small in comparison with the freestream velocity. Hayes[1] demonstrated that if in comparison with the streamwise velocity, the crossflow velocity and its derivatives are neglected, the two momentum equations are uncoupled in streamline coordinates, and additionally the crossflow momentum equation is linear.

However, the small crossflow assumption breaks down when the skew of the surface shear stress off of the inviscid streamline coordinate exceeds about 25–30°. Rainbird et al.[2] compared analytical and experimental results for a 12½° cone in incompressible flow, showing that above angles of skew of about 25° the small crossflow assumption becomes progressively less accurate. A similar conclusion can be reached from the analytical work of Fannelop[3] and Chan.[4] Each of these investigators used a perturbation technique to solve the general boundary-layer equations. Cumpsty and Head[5] reached the same conclusion in a study of the incompressible turbulent boundary layer. Dwyer[6] and Der[7] point out that the small crossflow assumption can be inaccurate even when the crossflow is small. Examples are the regions near the windward and leeward meridian of a body of revolution at angle of attack. The crossflow derivatives may not be negligible in this region.

Der[7] and Cooke[8] used numerical methods to examine the three-dimensional cone boundary layer. Results were presented for angles of attack up to approximately one cone half angle. In particular, Der suggests that the small crossflow assumption is invalid at an angle of attack on the order of one cone half angle. An approximate analysis of the laminar boundary layer is presented in this paper, and utilized to investigate the conditions at angles of attack much greater than one cone half angle. Numerical evaluations are given for 10° half-angle cones up to angles of attack of 24°, and 5° half-angle cones up to angles of attack of 55°. The results are found to compare favorably with the experimental data of Tracy[9] and Feldhuhn and Pasiuk[10] for 10 and 5° half-angle cones, respectively.

General Equations

A general curvilinear coordinate system was used to write the boundary-layer equations for steady flow. In this coordinate system an element of length dL is

$$(dL)^2 = (h_1 d\xi)^2 + (h_2 d\eta)^2 + (d\zeta)^2$$

where ξ, η are coordinates in the surface of the cone and ζ is a distance measured normal to the cone surface. The metric coefficients or scale factors h_1 and h_2 were assumed to be independent of ζ.

For $Pr = 1$, the compressible laminar boundary-layer equations are,[11]

Continuity

$$(\partial/\partial\xi)(\rho h_2 u) + (\partial/\partial\eta)(\rho h_1 v) + h_1 h_2 (\partial/\partial\zeta)(\rho w) = 0 \quad (1a)$$

Momentum

$$\rho(Du/Dt - uvK_2 + v^2 K_1) = -(1/h)\partial p/\partial\xi + (\partial/\partial\zeta)(\mu\partial u/\partial\zeta) \quad (1b)$$

$$\rho(Dv/Dt + u^2 K_2 - uvK_1) = -(1/h_2)\partial p/\partial\eta + (\partial/\partial\zeta)(\mu\partial v/\partial\zeta) \quad (1c)$$

Energy

$$\rho \frac{DH}{Dt} = \frac{\partial}{\partial\zeta}\left(\mu \frac{\partial H}{\partial\zeta}\right) \quad (1d)$$

where the operator D/Dt is defined by

$$D/Dt = (u/h_1)\partial/\partial\xi + (v/h_2)\partial/\partial\eta + w\partial/\partial\zeta$$

and

$$K_1 = -(1/h_1 h_2)\partial h_2/\partial\xi, \quad K_2 = -(1/h_1 h_2)\partial h_1/\partial\eta$$

These equations were solved by an approximate scheme which uses the so-called integral equations. The integral equations were obtained in the usual fashion of integrating across the boundary layer. First, however, a simple transformation was adopted which eliminates the variable density from the equations. A transformed variable was defined by

$$\bar{\zeta} = (C)^{-1/2} \int_0^\zeta \frac{\rho}{\rho_o} d\zeta \quad (2)$$

where the subscript o indicates a reference state taken here as the inviscid conditions at the windward meridian. Using the temperature at the boundary-layer edge and the cone surface, the parameter C was evaluated by the Sutherland temperature-viscosity relation. The variable density was thus eliminated from Eq. (1), and the form was similar to that of an incompressible flow. A complete transformation into the form of an incompressible flow is not possible because of the presence of heat transfer.

The transformed equations were then integrated over the limits, $\bar{\zeta} = 0$ to $\bar{\zeta} \to \infty$. Using the continuity equation to eliminate the transformed w velocity component, and using the thickness parameters defined in Appendix A, the resulting equations were

$$\frac{1}{h_1}\frac{\partial}{\partial\xi}(u_e^2\bar{\theta}_{11}) + \frac{1}{h_2}\frac{\partial}{\partial\eta}(u_e^2\bar{\theta}_{12}) - u_e^2 K_2(\bar{\theta}_{12} + \bar{\theta}_{21}) + -u_e^2 K_1(\bar{\theta}_{11} - \bar{\theta}_{22}) + \frac{u_e}{h_1}\frac{\partial u_e}{\partial\xi}\left[\left(1 + \frac{\gamma-1}{2}M^2\right)\times(\bar{\delta}_1 + \bar{\delta}_S) + \frac{\gamma-1}{2}M^2(\bar{\theta}_{11} + \bar{\theta}_{22})\right] + \frac{u_e}{h_2}\frac{\partial u_e}{\partial\eta}\bar{\delta}_2 = \frac{p}{p_o}\nu_o\left.\frac{\partial u}{\partial\bar{\zeta}}\right|_w \quad (3a)$$

$$\frac{1}{h_1}\frac{\partial}{\partial\xi}(u_e^2\bar{\theta}_{21}) + \frac{1}{h_2}\frac{\partial}{\partial\eta}(u_e^2\bar{\theta}_{22}) - K_1u_e^2(\bar{\theta}_{21} + \bar{\theta}_{12} + \bar{\delta}_2) + u_e^2K_2\left[\left(1 + \frac{\gamma-1}{2}M^2\right)(\bar{\delta}_1 + \bar{\delta}_S + \bar{\theta}_{11}) - \left(1 - \frac{\gamma-1}{2}M^2\right)\bar{\theta}_{22}\right] = \frac{p}{p_o}\nu_0\left.\frac{\partial v}{\partial\bar{\zeta}}\right|_w \quad (3b)$$

$$\frac{1}{h_1}\frac{\partial}{\partial\xi}(u_e\bar{\Theta}_1) + \frac{1}{h_2}\frac{\partial}{\partial\eta}(u_e\bar{\Theta}_2) - K_1\bar{\Theta}_1 - K_2\bar{\Theta}_2 = -\frac{p}{p_o}\nu_o\left.\frac{\partial S}{\partial\bar{\zeta}}\right|_w \quad (3c)$$

where $S = H/H_e - 1$. Equations (3) can provide a solution to three free parameters, so it was necessary to express the nine thickness parameters in terms of only three free parameters. This of course means the two velocity profiles and the total enthalpy profile had to be expressed with no more than three free parameters.

Streamlines on a Cone at Angle of Attack

As defined earlier, the coordinates ξ, η were restricted to the cone surface, but were otherwise unspecified. If the coordinates are taken as streamline coordinates, then Eqs. (3) represents a set of coupled partial differential equations. A solution could be obtained by an iterative process, whereby one neglects the derivatives with respect to η as a first iteration, and then includes approximations to these derivatives after a number of adjacent streamlines are computed. This procedure was demonstrated by Kang, et al.[12] for the case of an Apollo-type re-entry body. Because of the conical external flow, the problem could easily be formulated in a spherical coordinate system as well as in streamline coordinates. The streamline coordinates were chosen in this analysis because it is in such intrinsic coordinates that the behavior of the crossflow is best understood. This was considered an important advantage when modeling the crossflow velocity profile.

The coordinates of these streamlines and the direction cosines of the streamlines were determined from the pressure distribution. Using index notation for the inviscid velocity vector on the cone surface

$$u^k = u_e\lambda^k, \quad (k = 1,2)$$

where

$$\lambda^1 = \partial R/\partial s^1, \quad \lambda^2 = \partial\phi/\partial s^2 \quad (4)$$

Leigh and Ross[13] derived the differential equation for the unit vector λ^k for the case of a blunted cone. For the conical flow associated with the pointed cone, $p = p(\phi)$ only. The streamline direction cosines are also functions of ϕ only, and are expressed in terms of λ^k by

$$l = \lambda^1, \quad m = R\sin\theta_c\lambda^2 \quad (5)$$

Applying the chain rule for the partial derivatives in the streamwise direction

$$\partial/\partial s^1 = \lambda^1(\partial/\partial R) + \lambda^2(\partial/\partial\phi) \quad (6)$$

the equation of Leigh and Ross[13] reduces to

$$dl/d\bar{\phi} = m + lG(\bar{\phi}), \quad l^2 + m^2 = 1 \quad (7)$$

where $\bar{\phi} = \phi\sin\theta_c$ and

$$G(\bar{\phi}) = (1/\gamma pM^2)\partial p/\partial\bar{\phi}$$

Equation (7) was solved to give the local streamline properties. The coordinates of a streamline could be determined using Eq. (4) and the results from Eq. (7). From the analysis of

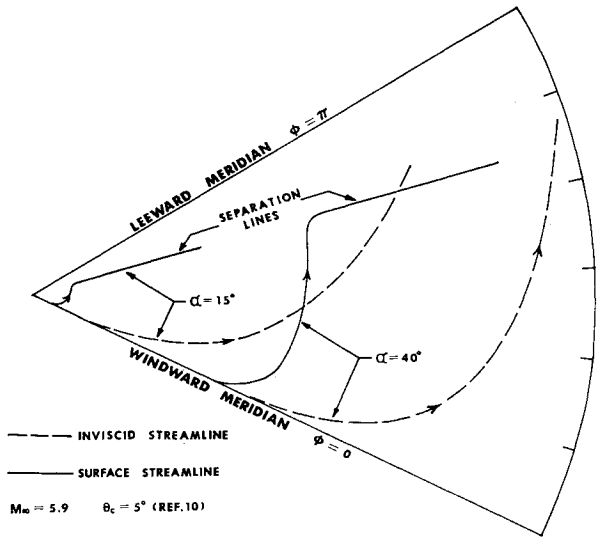

Fig. 2 Examples of inviscid and surface streamlines on the developed surface of a cone.

Leigh and Ross the curvature terms were determined to be

$$K_1 = l^2G(\bar{\phi})/mR, \quad K_2 = -lG(\bar{\phi})/R$$

The resulting inviscid streamlines based on the experimental pressure data of Feldhuhn and Pasiuk[10] for a 5° half-angle cone are shown in Fig. 2 for 15° and 40° angle of attack. Also shown are the surface streamlines based on the surface shear stress. The surface streamlines were based on oil drop flow visualization data of Feldhuhn and Pasiuk. The large difference between the surface and the inviscid streamline direction is apparent. The separation line was taken to be a cone ray and the surface streamline is tangent to this separation line. This is consistent with Maskell's[14] explanation of three-dimensional separation.

Assumed Profiles

Having adopted an approximate integral method, the choice of profiles was quite important. Based on favorable results obtained in incompressible flow with streamline inflection points, the following profiles of Cooke[15] were chosen:

$$u/u_e = f(z) - \Lambda g(z) \quad (8a)$$

$$v/u_e = \Pi h(z) - Ng(z) \quad (8b)$$

where

$$z = \bar{\zeta}(\nu_0\sigma)^{-0.5}$$

$$f(z) = 1 - (2/\pi^{0.5})ze^{-z^2} - \mathrm{erfc}(z)$$

$$g(z) = e^{-z^2}(z/3\pi^{0.5} - \tfrac{1}{2}) - \tfrac{1}{2}\mathrm{erfc}(z)$$

$$h(z) = ze^{-z^2}$$

In these profiles σ and Π are free parameters evaluated in the solution of the differential equations. N and Λ were determined from the so-called compatibility conditions fixed by the wall boundary conditions, $u = v = 0$, to be

$$\Lambda = -(1 + S_w)\left(1 + \frac{\gamma-1}{2}M^2\right)\sigma\lambda^2\bar{u}_eG(\phi)/\bar{p}$$

$$N = (1 - S_w)\left(1 - \frac{\gamma-1}{2}M^2\right)\sigma K_2\bar{u}_e/\bar{p}$$

The two-parameter family of streamwise velocity profiles is commonly used in problems involving adverse pressure. The additional free parameter Π introduced in the cross-

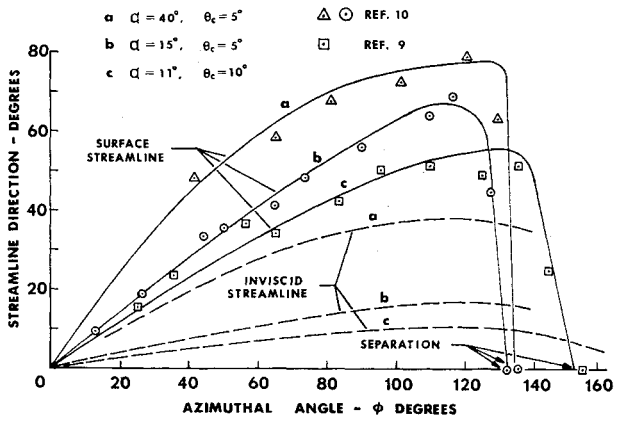

Fig. 3 Comparison of surface streamline results with experimental data.[9,10]

flow velocity profile, allowed the possible existence of s shaped profiles, and allowed the crossflow velocity to be nonzero when the curvature K_2 was zero. K_2 is zero at the point of minimum pressure, however, the crossflow is quite large here. A profile which assumed zero velocity at this point could be expected to introduce a significant error.

The total enthalpy profile contained a free parameter which determined the heat transfer rate, and satisfied the boundary condition $S \to 0$ as $z \to \infty$ and $S = S_w$ at $z = 0$. The profile formulated for this analysis was

$$S/S_w = 1 - f(z) - \chi h(z) \tag{9}$$

where χ is the free parameter.

Solution of Integral Equation

Just as Eq. (6) represents a transformation from streamline coordinate derivative to spherical coordinate derivative, a similar equation can be utilized for the derivative with respect to the streamline normal coordinate. Again applying the chain rule to a partial derivative gives

$$(1/h_2)\partial/\partial\eta = \partial/\partial s^2 = \eta^1(\partial/\partial R) + \eta^2(\partial/\partial\phi)$$

Using the fact that η^k is normal to λ^k, η^k can be eliminated in favor of λ^k to yield

$$\frac{\partial}{\partial s^2} = -\lambda^2 R \sin\theta_c \frac{\partial}{\partial R} + \frac{\lambda^1}{R \sin\theta_c} \frac{\partial}{\partial\phi} \tag{10}$$

Eqs. (6) and (10) were then applied to the integral equation, Eq. (3). The thickness parameters were evaluated using the assumed profiles of Eqs. (8) and (9). The dimensionless parameter $\Sigma = \sigma u_o/R$ was defined, and the thickness parameters were assumed to grow according to $R^{0.5}$. This allowed the explicit appearance of R to disappear and after algebraic manipulation the below set of nonlinear first-order ordinary differential equations resulted for the free parameters Σ, Π, and χ

$$F_1 \frac{d\Sigma}{d\bar{\phi}} + F_2 \frac{d\Pi}{d\bar{\phi}} + F_4 = 0$$

$$G_1 \frac{d\Sigma}{d\bar{\phi}} + G_2 \frac{d\Pi}{d\bar{\phi}} + G_4 = 0 \tag{11}$$

$$H_1 \frac{d\Sigma}{d\bar{\phi}} + H_2 \frac{d\Pi}{d\bar{\phi}} + H_3 \frac{d\chi}{d\bar{\phi}} + H_4 = 0$$

The coefficients F_i, G_i and H_i are listed in Appendix B.

The free parameters Σ, Π, and χ can be determined by integrating Eq. (11) once the pressure distribution is known. Tracy[9] and Feldhuhn and Pasiuk[10] have studied experimentally the surface pressure distribution and other properties on cones at high angles of attack. This provided an evaluation of the approximate method by comparing the integrated results for wall shear stress and heat transfer with the experimental data.

The integration began just off the windward meridian. Starting values for Σ and χ were determined from an independent solution of the equations determined by Reshotko[16] for the windward meridian of an inclined cone. The starting value of Π was zero, since the crossflow is identically zero on the windward meridian. Because these initial values did not satisfy exactly the governing equations the first few steps of the integration produced oscillatory results. If this oscillation diverged, the solution was restarted somewhat further off of the windward meridian. Working in this manner, no solution was started further than 0.02 rad off the windward meridian. Using integration steps of 0.005 rad, a complete calculation up to the separation line using a fourth-order Runge-Kutta procedure required about 40 sec on an IBM 7094 system. The lower angles of attack were computed accurately using a step size of 0.01 rad. On the other hand, when the angle of attack exceeded 50°, a step size of 0.002 rad was often used, and the computations did not extend beyond the point of minimum pressure. At these high angles of attack, instability invariably occurred in the region of adverse pressure, and the separation point was not determined.

Surface Streamlines

The surface streamline direction is identical to the direction of the local surface shear stress. In terms of the skin-friction coefficient, the streamwise and crossflow components of wall shear stress are

$$c_{fs}(Re/C)^{0.5} = a_1(2 + \Lambda)\bar{u}_e\bar{\rho}/\Sigma^{0.5}$$

$$c_{fn}(Re/C)^{0.5} = (2\Pi + a_1 N)\bar{u}_e\bar{\rho}/\Sigma^{0.5}$$

The local value of the direction of the surface streamlines was determined from the direction of the shear stress components and compared with experimental results on 5°[10] and 10°[9] half angle cones. A favorable comparison was found in-

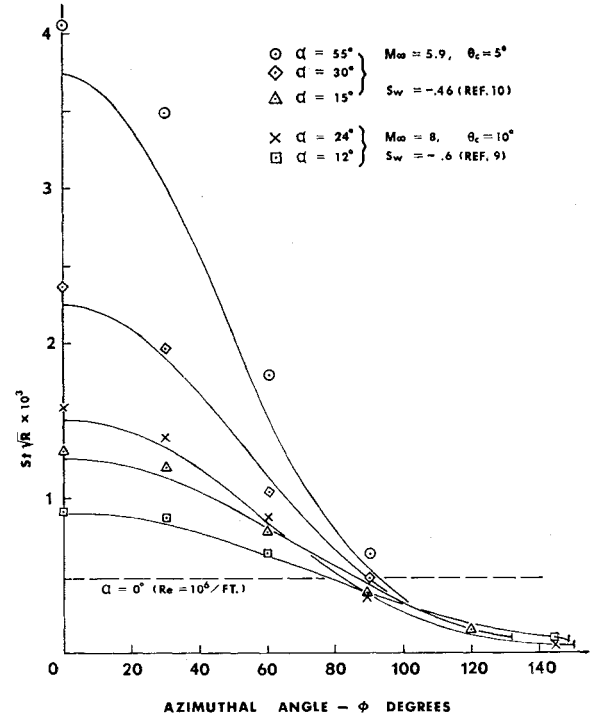

Fig. 4 Comparison of Stanton number results with experimental data.[9,10]

cluding the prediction of the separation line, as noted in Fig. 3. It is interesting that the difference between the directions of the surface streamline and the inviscid streamline coordinate direction is greater at an angle of attack of 15° than at 40° angle of attack on the 5° half-angle cone. Another significant feature of these results is the great change in the direction of the streamlines just prior to the separation point. The flow near the wall undergoes a large reversal in the direction while near the edge of the boundary layer the change in direction is small. This illustrates the need for two parameter crossflow velocity profiles in this region.

Heat Transfer

The local Stanton number was computed for a determination of wall heat flux. Using the free parameter χ of the analysis the local Stanton number is found to be

$$St(Re/C)^{0.5} = (a_1 + \chi)\bar{p}/\Sigma^{0.5}$$

for unit Prandtl number. The computed results are compared with the data of Tracy[9] and with Feldhuhn and Pasiuk in Fig. 4. Tracy's results were referenced to the zero angle-of-attack value of the cone Stanton number. In this analysis, the reference value of Stanton number was based on the flat plate data of Van Driest,[17] and computed for the flow conditions of Tracy's experiment. For $Pr = 1$, the result was $St(Re)^{0.5} = 0.484$. The comparison of the analytical results with the experimental data was again found to be good.

Crossflow

The influence of wall temperature on the magnitude of crossflow is well known. Vaglio-Laurin[18] pointed out that when the quantity $(u/u_e)^2 - \rho_e/\rho$ is zero, the crossflow measured in streamline coordinates is identically zero. This condition on the velocity profile is known to be approximated for very cold walls and high hypersonic Mach numbers. A reduction in the skew of the surface streamline off the inviscid streamline direction as the wall temperature becomes colder is clearly seen in the surface streamline results of Fig. 5. Various crossflow velocity profiles plotted in Fig. 6 also illustrates this point.

Another important feature of the crossflow is the significance of the free parameter II in Eq. (8b), the assumed crossflow velocity profile. The wall compatibility condition requires the form parameter N in Eq. (8b) to be dependent on the pressure gradient. Thus N is zero at the pressure minimum. However, as shown in Fig. 6, the crossflow velocity is quite large at this point. In the region of the adverse pressure gradient, reversal of the crossflow begins. This most influences the fluid near the wall, where a reversal in the crossflow velocity occurs. If separation is sufficiently delayed the entire profile eventually reverses. To predict such behavior the crossflow velocity profile must be a two parameter family.

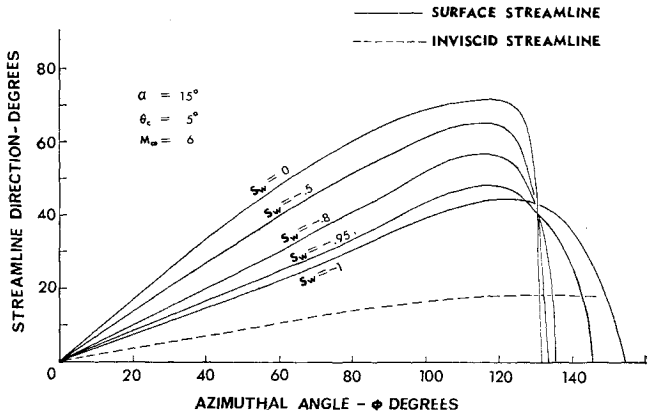

Fig. 5 The effect of wall temperature on surface streamline direction.

The results of Fig. 5 indicate that the separation point is not moved downstream significantly until S_w becomes less than about -0.8. The experimental pressure distribution[10] used to obtain these results is valid on the leeward side for moderately cold walls ($S_w = -0.5$). Since the separation point moves significantly, the pressure distribution on the leeward side is affected. For this reason, the large change in the separation point for $S_w = -0.95$ and $S_w = -1$ should be considered only qualitatively correct.

Boundary Layer and Displacement Thickness

In two-dimensional flow, the displacement thickness is defined by

$$\delta_1 = \int_0^\infty \left(1 - \frac{\rho u}{\rho_e u_e}\right) d\zeta$$

However, for a three-dimensional boundary layer Lighthill[19] noted that the displacement effect of mass entrainment from the freestream is inadequate for the definition of a true

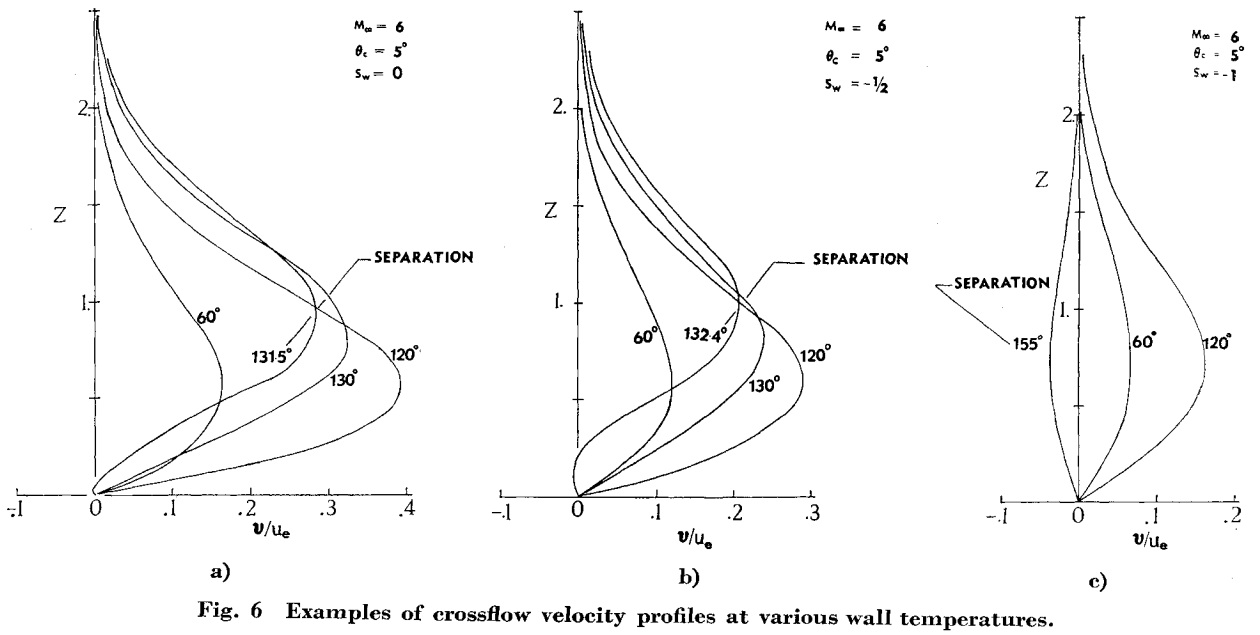

Fig. 6 Examples of crossflow velocity profiles at various wall temperatures.

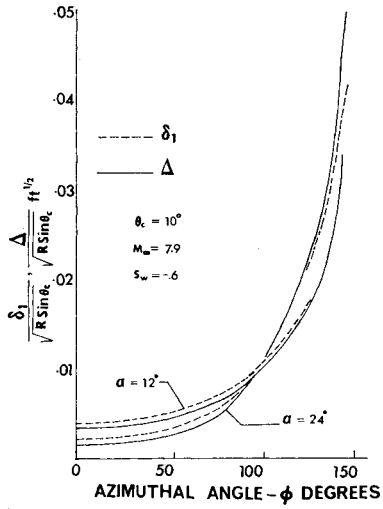

Fig. 7 Growth of displacement thickness on a cone at high angle of attack.

displacement thickness. If a crossflow exists, the net effect of a change of the crossflow along a streamline must be considered. Thus if the crossflow increases along a streamline, the effect of mass entrainment is somewhat lessened. On the other hand, if the crossflow is decreasing, the entrainment effect is augmented.

Lighthill accounted for these phenomena and determined a three-dimensional displacement thickness by

$$\Delta = \delta_1 - \frac{1}{\rho_e u_e h_2} \frac{\partial}{\partial \eta} \int_0^\xi \rho_e u_e \delta_2 h_1 d\xi$$

The second term of this expression was evaluated for the case of a cone at angle of attack, giving

$$\Delta = \delta_1 - \frac{\rho_o}{\rho_e}\left[\frac{2}{3} l^2 \frac{\partial \delta_2}{\partial \bar{\phi}} - \frac{2}{3} lm\delta_2 - \frac{3}{2}\frac{m}{u_e}\int_0^{\bar{\phi}} mu_e\delta_2 d\bar{\phi}\right]$$

Typical behavior of the displacement thickness is plotted in Fig. 7. The three dimensional displacement thickness Δ was less than the streamwise displacement thickness δ_1 on the windward side where the crossflow is growing. However, in the region of the pressure minimum the magnitude of the crossflow decreases somewhat and the three-dimensional displacement thickness began to grow rapidly and at high angle of attack it became greater than the streamwise displacement thickness. The displacement thickness predicted by the windward meridian analysis of Reshotko[16] is noted in Table 1. The approximate method gave significantly lower values. At high angles of attack ($\alpha > 40°$) on the 5° half angle cone the approximate method gave negative values for the three-dimensional displacement thickness. Although such negative values are possible due to a rapid growth in crossflow, the negative values of Δ encountered in this analysis are believed to be caused by the low predicted value of the streamwise displacement thickness. At approximately 30° off of the windward meridian the three-dimensional displacement thickness was no longer negative.

Using the transformation, Eq. 2, and by defining the boundary-layer edge as the location where $u/u_e = 0.99$, the boundary-layer thickness was calculated at the separation point. Predicted boundary-layer thickness is compared in Table 2 with experimental data presented by Tracy[9] which was based on pitot pressure surveys. As seen from this comparison the computed results are approximately 25% lower than the experimental data.

Conclusions

Using an approximate integral method, a laminar three-dimensional boundary-layer solution including convective heat transfer and not restricted to small crossflow and irrotational external flow has been obtained. The computations show that except for wall temperature parameter S_w greater than about -0.8, the small crossflow assumption is invalid for angles of attack in excess of the cone half angle.

Comparison with experimental data in the literature show that heat transfer and surface shear stress can be predicted accurately. However, the computations for displacement and boundary-layer thickness appear to yield lower values compared to data in the literature.

Appendix A: Thickness Parameters

In the transformed coordinate the following parameters were used

$$\bar{\delta}_1 = \int_0^\infty \left(1 - \frac{u}{u_e}\right) d\bar{\zeta},\ \bar{\delta}_2 = -\int_0^\infty \frac{v}{u_e} d\bar{\zeta}$$

$$\bar{\delta}_s = -\int_0^\infty S d\bar{\zeta},\ \bar{\theta}_{11} = \int_0^\infty \left(1 - \frac{u}{u_e}\right)\frac{u}{u_e} d\bar{\zeta}$$

$$\bar{\theta}_{12} = \int_0^\infty \left(1 - \frac{u}{u_e}\right)\frac{v}{u_e} d\bar{\zeta},\ \bar{\theta}_{21} = -\int_0^\infty \frac{uv}{u_e^2} d\bar{\zeta}$$

$$\bar{\theta}_{22} = -\int_0^\infty \frac{v^2}{u_e^2} d\bar{\zeta},\ \bar{\Theta}_1 = \int_0^\infty S\frac{u}{u_e} d\bar{\zeta},\ \bar{\Theta}_2 = \int_0^\infty S\frac{v}{u_e} d\bar{\zeta}$$

Using the transformation equation, Eq. (2), the streamwise displacement thickness in physical coordinates is found to be

$$\delta_1 = \frac{C^{0.5}}{\bar{\rho}_e}\left[\left(1 + \frac{\gamma - 1}{2} M^2\right)(\bar{\delta}_1 + \bar{\delta}_S) + \frac{\gamma - 1}{2} M^2 (\bar{\theta}_{11} + \bar{\theta}_{22})\right]$$

All other thickness parameters in physical coordinates are found by multiplying the analogous parameter in transformed coordinates by $C^{0.5}/\bar{\rho}_e$. Thus, for example

$$\delta_2 = \bar{\delta}_2\, C^{0.5}/\bar{\rho}_e$$

Appendix B: Coefficients

The coefficients of Eq. (11) are listed below.

$$F_1 = r_1 + r_2\Sigma + r_3\Sigma^2 + r_4\Pi\Sigma + r_5\Pi,\ F_2 = 2r_5\Sigma + 2/3r_4\Sigma^2$$

$$F_4 = r_6\Sigma + r_7\Sigma^2 + r_8\Sigma^3 + r_9\Pi\Sigma + r_{10}\Pi\Sigma^2 + r_{11}\Pi^2\Sigma + r_{12}\Sigma\chi + r_{13}$$

$$G_1 = r_{14}\Sigma + r_{15}\Sigma^2 + r_{16}\Pi\Sigma + r_{17}\Pi + r_{18}\Pi^2$$

$$G_2 = 2r_{17}\Sigma + 2/3r_{16}\Sigma^2 + 4r_{18}\Pi\Sigma$$

Table 1 Displacement thickness on the windward meridian, $\theta_c = 10°$, $S_w = -0.6$, $M_\infty = 7.9$

	$\delta_1(3u_o/C\nu_o R)^{1/2}$		$\Delta(3u_o/C\nu_o R)^{1/2}$	
α	Exact[16]	Approximate	Exact[16]	Approximate
12°	6.627	3.665	6.200	3.005
24°	3.079	1.685	2.797	1.102

Table 2 Boundary-layer thickness at the separation point, $\theta_c = 10°$, $S_w = -0.6$, $M_\infty = 7.9$

	$\delta/(R\sin\theta_c)^{1/2}$	
α	Computed	Experiment[9]
12°	0.0480	0.0646
24°	0.0632	0.0858

$$G_4 = r_{19}\Sigma + r_{20}\Sigma^2 + r_{21}\Sigma^3 + r_{22}\Pi^2\Sigma + r_{23}\Pi\Sigma^2 + r_{24}\Pi\Sigma + r_{25}\Pi + r_{26}\Sigma\chi$$

$$H_1 = r_{27}\Sigma + r_{28}\Sigma\chi + r_{17}\chi + r_{18}\Pi\chi + r_5\Pi + r_1$$

$$H_2 = 2r_5\Sigma + 2r_{18}\Sigma\chi, \; H_3 = 2r_{17}\Sigma + 2/3r_{28}\Sigma^2 + 2r_{18}\Sigma\chi$$

$$H_4 = r_{29}\Sigma + r_{30}\Sigma^2 + r_{31}\Sigma\chi + r_{32}\Sigma^2\chi + r_{33}\Pi\Sigma\chi + r_9\Pi\Sigma + r_{34}\chi - r_{13}$$

where

$$r_1 = 0.5a_8m, \; r_2 = 1.5Y[a_4 + (a_4 + a_2)m^2]$$

$$r_3 = 2.5a_7Y^2m, \; r_4 = 1.5a_6Ylm, \; r_5 = 0.5a_5l$$

$$r_6 = -a_8[G/m + \{1 + F(M)\}Gm] - 0.5a_1Ym\bar{p}/\bar{u} - a_1(1 + S_w)[1 + F(M)]Gm$$

$$r_7 = (a_4 + a_2)[0.5Ylm + m^2dY/d\bar{\phi} - 2YG - \{1 + F(M)\}YGm^2] + a_4(dY/d\bar{\phi} - YG)$$

$$r_8 = a_7[2YmdY/d\bar{\phi} - Y^2l - \{2 + F(M)\}Y^2Gm^2]$$

$$r_9 = -0.5a_5m, \; r_{10} = a_6[mldY/d\bar{\phi} - 0.5Ym^2 - Yl^2 + Yl^3G/m - 2F(M)YGlm]$$

$$r_{11} = a_9[Gl^2/m - F(M)Gm], \; r_{12} = -a_3S_w[1 + F(M)]Gm$$

$$r_{13} = -a_1\bar{p}/\bar{u}, \; r_{14} = 1.5(a_4 + a_2)Ylm, \; r_{15} = 2.5a_7Y^2l$$

$$r_{16} = 1.5a_6Y(1 + l^2), \; r_{17} = 0.5(a_5 + a_3)m, \; r_{18} = 0.5a_9l$$

$$r_{19} = 1.5(a_4 + a_2)Ylm - [1 + F(M)] \times [a_8 + (1 + S_w)a_1]Gl$$

$$r_{20} = 2.5a_7Y^2l^2m + (a_4 + a_2)[Ym^2 - Yl^2 + lmdY/d\bar{\phi} - 2Yl^3G/m - \{1 + F(M)\}YGlm]$$

$$r_{21} = a_7[Y^2m(1 - 2.5l^2) + 2YldY/d\bar{\phi} - \{2 + F(M)\}Y^2Gl]$$

$$r_{22} = a_9[0.5m - \{1 + F(M)\}Gl]$$

$$r_{23} = a_6[(1 + l^2)dY/d\bar{\phi} - Ylm - 2YG - \{1 + 2F(M)\}YGl^2]$$

$$r_{24} = 1.5a_6Ylm - 2(a_5 + a_3)G/m, \; r_{25} = 0.5(a_5 + a_3) - \bar{p}/\bar{u}$$

$$r_{26} = -a_3S_w[1 + F(M)]Gl, \; r_{27} = 1.5a_6Y, \; r_{28} = 1.5a_6Y$$

$$r_{29} = a_8(0.5l - G/m), \; r_{30} = a_4(dY/d\bar{\phi}YG)$$

$$r_{31} = (a_5 + a_3)(0.5l - G/m), \; r_{32} = a_6(dY/d\bar{\phi} - YG)$$

$$r_{33} = -0.5a_9m, \; r_{34} = -\bar{p}/\bar{u}$$

and

$$a_1 = 0.752253, \; a_2 = -0.066987, \; a_3 = -0.500000$$

$$a_4 = 0.037161, \; a_5 = 0.205372, \; a_6 = -0.022314$$

$$a_7 = -0.003798, \; a_8 = 0.289430, \; a_9 = -0.156668$$

References

[1] Hayes, W. D., "The Three-Dimensional Boundary Layer," NAVORD Rept. 1313, NOTS 384, May 9, 1951, U.S. Naval Ordnance Test Station, China Lake, Calif.

[2] Rainbird, W. J., Crabbe, R. A., and Jurewicz, L. S., "A Water Tunnel Investigation of the Flow Separation About Circular Cones at Incidence," AERO Rept. LR-385, Sept. 1963, National Research Council of Canada, Ottawa.

[3] Fannelop, T. K., "A Method of Solving the Three-Dimensional Laminar Boundary-Layer Equations with Application to a Lifting Re-entry Body," *AIAA Journal*, Vol. 6, No. 6, June 1968, pp. 1075–1084.

[4] Chan, Y. Y., "An Approximate Method for Three-Dimensional Compressible Laminar Boundary Layers with Small Crossflow," AERO Rept. LR-455, June 1966, National Research Council of Canada, Ottawa.

[5] Cumpsty, N. A. and Head, M. R., "The Calculation of Three-Dimensional Turbulent Boundary Layers, Part I, Flow Over the Rear of An Infinite Swept Wing," *Aeronautical Quarterly*, Vol. 18, Part 1, Feb. 1967, pp. 55–84.

[6] Dwyer, H. A., "Solution of a Three-Dimensional Boundary-Layer Flow with Separation," *AIAA Journal*, Vol. 6, No. 7, July 1968, pp. 1336–1342.

[7] Der, J., Jr., "A Study of General Three-Dimensional Boundary Layer Problems by an Exact Numerical Method," AIAA Paper 69-138, New York, 1969.

[8] Cooke, J. C., "Supersonic Laminar Boundary Layers on Cones," TR 66347, Nov. 1966, Royal Aircraft Establishment, Farnborough, England.

[9] Tracy, R. R., "Hypersonic Flow Over a Yawed Cone," Memo 69, Aug. 1, 1963, Graduate Aeronautical Labs., California Institute of Technology, Pasadena, Calif.

[10] Feldhuhn, R. H., and Pasiuk, L., "An Experimental Investigation of the Aerodynamic Characteristics of Slender Hypersonic Vehicles at High Angles of Attack," NOLTR68-52, May 1, 1968, U.S. Naval Ordnance Lab., White Oak, Md.

[11] Mager, A., *Theory of Laminar Flows*, Pt. C, edited by F. K. Moore, Princeton University Press, 1964.

[12] Kang, S. W., Rae, W. J., and Dunn, M. G., "Studies of Three-Dimensional Compressible Boundary Layers on Blunt Lifting Entry Bodies," *AGARD Conference Proceedings*, No. 30, May 1968, 7 Rue Ancelle, 92 Neuilly-sur-Seine, France.

[13] Leigh, D. C. and Ross, B. B., "Surface Geometry on Three-Dimensional Inviscid Hypersonic Flows," *AIAA Journal*, Vol. 7, No. 1, Jan. 1969, pp. 123–129.

[14] Maskell, E. C., "Flow Separation in Three Dimensions," Rept. Aero 2565, 1955, Royal Aircraft Establishment, Farnborough, England.

[15] Cooke, J. C., "Approximate Calculation of Three-Dimensional Laminar Boundary Layers," R and M 3201, Oct. 1959, Aeronautical Research Council, England.

[16] Reshotko, E., "Laminar Boundary Layer with Heat Transfer on a Cone at Angle of Attack in a Supersonic Stream," TN 4152, Dec. 1957, NACA.

[17] Van Driest, E. R., "Investigation of the Laminar Boundary Layer in Compressible Fluids Using the Crocco Method," TN 2597, 1952, NACA.

[18] Vaglio-Laurin, R., "Laminar Heat Transfer on Three-Dimensional Blunt Nosed Bodies in Hypersonic Flow," *ARS Journal*, Vol. 29, Feb. 1959, pp. 123–129.

[19] Lighthill, M. J., "On Displacement Thickness," *Journal of Fluid Mechanics*, Vol. 2, Pt. 2, 1958, pp. 383–392.